One Earth

Article

Reforestation increases water inequality under low warming but reduces water availability under high warming

Graphical abstract

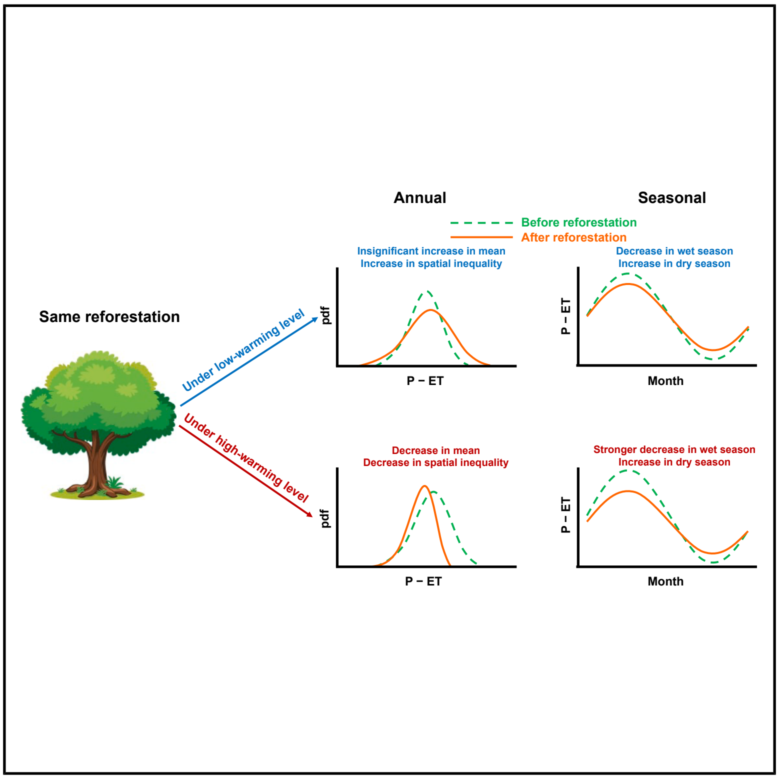

Highlights

- Reforestation impacts on water availability differ under two emission scenarios
- The study fully accounts for indirect effects and feedbacks from land use change
- Water availability responses diverge between low- and high-warming scenarios

Authors

Tao Tang, Jun Ge, Haiyun Shi, Junji Cao, Xuhui Lee

Correspondence

tangtao@mail.iap.ac.cn (T.T.), jjcao@mail.iap.ac.cn (J.C.)

In brief

We find that the same reforestation has distinct impacts on water availability under different background climates, not only in the mean amount but also in spatial and seasonal distributions. This highlights that the hydrological outcomes of reforestation are pathway-dependent—a key insight for policymakers.

Tang et al., 2026, One Earth *9*, 101740
August 21, 2026
https://doi.org/10.1016/j.oneear.2026.101740

CellPress

Please cite this article in press as: Tang et al., Reforestation increases water inequality under low warming but reduces water availability under high warming, One Earth (2026), https://doi.org/10.1016/j.oneear.2026.101740

One Earth

CellPress
OPEN ACCESS

Article

Reforestation increases water inequality under low warming but reduces water availability under high warming

Tao Tang,[1,6,*] Jun Ge,[2] Haiyun Shi,[3] Junji Cao,[4,*] and Xuhui Lee[5]
[1]State Key Laboratory of Earth System Numerical Modeling and Application, Institute of Atmospheric Physics, Chinese Academy of Sciences, Beijing 100029, China
[2]Joint International Research Laboratory of Atmospheric and Earth System Sciences, School of Atmospheric Sciences, Nanjing University, Nanjing 210023, China
[3]School of Environmental Science and Engineering, Southern University of Science and Technology, Shenzhen 518055, China
[4]State Key Laboratory of Atmospheric Environment and Extreme Meteorology, Institute of Atmospheric Physics, Chinese Academy of Sciences, Beijing 100029, China
[5]School of Environment, Yale University, New Haven, CT 06511, USA
[6]Lead contact
*Correspondence: tangtao@mail.iap.ac.cn (T.T.), jjcao@mail.iap.ac.cn (J.C.)
https://doi.org/10.1016/j.oneear.2026.101740

SCIENCE FOR SOCIETY Planting trees is often seen as a simple solution to climate change, but reforestation also affects water. It can change rainfall patterns and how much water is available for people, farms, and ecosystems. What we do not know is whether the same reforestation effort will have the same effect on water in a warmer future. Using climate models, we compared reforestation impacts under a low-warming scenario and a high-warming scenario. We found that under low warming, reforestation slightly increases global water but makes wet regions wetter, worsening water inequality. Under high warming, the same reforestation reduces global water availability. This matters because reforestation is not a one-size-fits-all solution. In a hotter world, planting trees may come with hidden water costs. Policymakers and the public need to know that where and when we plant trees matters just as much as how many we plant.

SUMMARY

Land management plays a critical role in climate mitigation and local water security. Reforestation, as a key land management strategy, is widely implemented to sequester carbon, and it also alters local water availability through biophysical effects. However, how the same reforestation activity affects water availability under different climate states remains unclear, a gap critical for adaptive land management and water policy. Here, we show that the hydrological consequences of reforestation depend on the background climate state. Using Earth system model simulations, we find that under a low-warming scenario, reforestation causes an insignificant increase in global mean water availability but increases spatial inequality (stronger wetting over wet regions). In contrast, under a high-warming scenario, reforestation reduces global water availability while weakening spatial inequality (drying over wet regions). A moisture budget analysis attributes these differences to circulation responses in wet regions. Our findings reveal that climate context shapes reforestation outcomes, providing practical insights for policymakers designing climate-adaptive land management strategies.

INTRODUCTION

Adaptive land management plays a critical role in climate mitigation and water security. Reforestation, as a key land management strategy, is widely implemented to sequester carbon.[1–5] Beyond carbon sequestration, forests also influence local and regional climate through biophysical effects—altering albedo, surface roughness, and evapotranspiration (ET)[6,7]—which collectively shape surface water and energy fluxes. Compared with other land cover types, forests typically enhance ET via deeper rooting, greater canopy interception, and more absorbed energy and have been shown to increase precipitation (P) locally and downwind, potentially alleviating surface dryness.[8–10] Consequently, large-scale reforestation programs, such as the

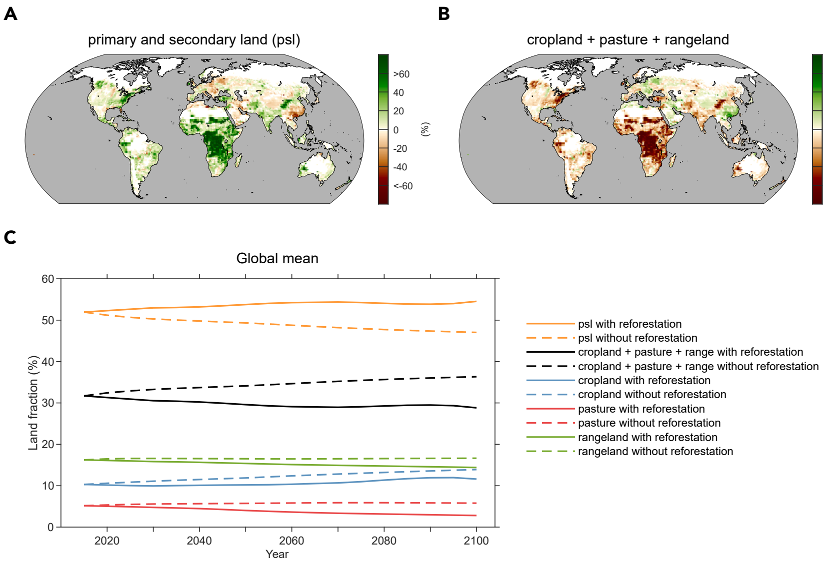

Figure 1. Land use and land cover changes
(A) Fractional changes of primary and secondary land (psl) due to reforestation.
(B) Concomitant changes of agricultural fields (combination of cropland, pasture, and rangeland).
(C) Time series of fractions for each land type with and without reforestation over 2015–2100, with solid (dashed) lines representing the reforestation (without reforestation) scenario.

Grain for Green Project in China, the Great Green Wall program in Africa, and the Bonn Challenge, have been implemented worldwide to combat desertification and ecosystem degradation. A critical outcome of these efforts is their impact on land water availability (defined as P-ET), which plays a vital role in maintaining life and providing essential ecosystem services.

However, published studies face three key limitations: incomplete treatment of indirect effects or feedback,[11–13] assumption of an unchanged background climate,[14,15] and a focus on regional or watershed scales[16,17] rather than the global scale. These gaps leave it unclear how large-scale reforestation will affect water availability on a global scale in a warmer world, especially when indirect effects and climate feedbacks are included.

Beyond these limitations, another critical but often overlooked issue is the background warming level itself. The same reforestation activity can lead to different temperature responses under different CO_2 concentrations.[18] A simple example is the albedo effect. Forests are darker than open land, and this contrast is more pronounced in winter when snow makes the open land brighter, particularly in mid-to-high latitudes.[19] In a warmer world, however, the reduced snow cover will reshape the surface energy budget, thereby affecting ET and P. This raises the possibility that the hydrological consequences of reforestation may also depend on the level of warming. It therefore remains unknown how the same reforestation activity would alter P-ET under different warming levels. Answering this question matters for two reasons. First, without accounting for climate-dependent feedbacks, we risk over- or underestimating the hydrological consequences of reforestation activity in a warmer world.[20–23] Second, understanding whether reforestation produces divergent P-ET responses under low versus high warming can inform adaptive land-management and water-policy decisions across different emission pathways. Here, we investigate the projected impacts of reforestation on P-ET under two contrasting warming levels using the latest Earth system model simulations. We find that the same reforestation effort leads to divergent effects on land water availability across different climate states, with implications for climate-smart reforestation design and water resource planning.

RESULTS

Reforestation under two different climate states

Four sets of model simulations participating in the Scenario Model Intercomparison Project[24] are employed in this study (see methods). The first two simulations are climate projections under the shared socioeconomic pathway (SSP)3-7.0 scenario (SSP370) and SSP1-2.6 scenario (SSP126), respectively. The SSP3-7.0 scenario represents a medium-to-high emission pathway, with continued deforestation at current rates and limited climate mitigation policies. The global mean temperature under this scenario is about 4 K warmer by 2100 relative to the 1850 level. The SSP1-2.6 represents a low-emission and sustainable pathway with strong climate mitigation policies, aiming to constrain the global mean temperature rise below 2 K by 2100. In the SSP1-2.6 scenario, forests are substantially recovered at the expense of agricultural fields (crop, pasture, and rangeland). The 3rd simulation is identical to the SSP370 simulation, but with land use and land cover change (LULCC) adapted from the SSP126 scenario (SSP370126Lu), which represents the reforestation version of SSP370. By taking the differences between these two simulations (SSP370126Lu minus SSP370), the impact of reforestation under the SSP3-7.0 could be isolated, denoted as $\delta(P\text{-}ET)_{ssp370}$. It is noted that the concentrations of greenhouse gases in both simulations are identical; thus, only biophysical effects related to changes in surface properties and associated atmospheric feedbacks are identified here. The 4th simulation is identical to the SSP126 simulation but with LULCC adapted from the SSP370 simulation (SSP126370Lu). The differences between these two simulations, SSP126 minus SSP126370Lu, represent the biophysical impacts of the same reforestation under the SSP1-2.6 scenario (denoted as $\delta(P\text{-}ET)_{ssp126}$). As the reforestation scenario in both comparisons is exactly the same (see Figure 1), by comparing the results from these two comparisons ($\delta(P\text{-}ET)_{ssp126}$ minus $\delta(P\text{-}ET)_{ssp370}$), the impact of the same reforestation activity under the two different warming levels could be obtained. Seven models that archive all four simulations are used in this study, and the results are presented as multi-model mean (MMM) values over the period of 2081–2100.

The changes in the spatial patterns of primary and secondary land (psl) and agricultural fields (the combination of cropland, pasture, and rangeland) due to reforestation are shown in Figure 1. The reforestation is seen almost worldwide, with the

Please cite this article in press as: Tang et al., Reforestation increases water inequality under low warming but reduces water availability under high warming, One Earth (2026), https://doi.org/10.1016/j.oneear.2026.101740

largest recovery of psl found in Africa. Globally, the psl covers 52.3% of the land (without Antarctica) in 2014. Without reforestation, the psl fraction will decrease to 47.0% by 2100, while reforestation will increase the psl fraction to 54.5% at the expense of agricultural fields. In other words, 7.5% of global land, amounting to ∼11 Mkm^2, is reforested or restored by 2100. At the same time, cropland (2.3%), pasture (3.0%), and rangeland (2.2%) decrease by the indicated fractions, respectively. It is also worth noting that the reforestation scenario identified here is based on the global mean change in the psl fraction. Deforestation also exists in the reforestation activity, such as East Europe and South China (Figure 1A).

Global and regional responses

To assess how background climate shapes reforestation impact on water availability, we first compare the spatial patterns of δ(P-ET) under the two scenarios on both global and regional scales (Figures 2A and 2B). The results are grouped into the 27 land regions,[25] with the full names of each region shown in Figure S1. The relative changes are shown in Figure S2. On the whole, reforestation under the SSP1-2.6 scenario causes an insignificant increase of 0.003 (–0.006 to 0.010) mm day^{-1} (MMM and 90% confidence interval [CI]) in P-ET globally, with 51.2% of the global land showing positive δ(P-ET). On the other hand, reforestation under the SSP3-7.0 scenario leads to a reduction in globally averaged P-ET, with an MMM value of −0.013 (–0.025 to –0.004) mm day^{-1}, which is statistically significant at the p = 0.10 level. In the latter case, 53.4% of the global land shows a drying response. Such differences are more pronounced in the distribution plot (Figure 2C), in which the distribution is skewed to the left (right) in the SSP3-7.0 (SSP1-2.6) scenario, demonstrating that more land fractions are drying (wetting) under the SSP3-7.0 (SSP1-2.6) scenario. Regionally, 14 out of the 27 land regions show positive δ(P-ET) due to reforestation under the SSP1-2.6 scenario, whereas only 9 regions show positive δ(P-ET) under the SSP3-7.0 scenario. By taking their differences (δ(P-ET)$_{ssp126}$ minus δ(P-ET)$_{ssp370}$), the different impacts of the same reforestation under these two scenarios are obtained, which are denoted by Δ(δ(P-ET)) and shown in Figure 2D. Specifically, 52.9% of the global land shows positive Δ(δ(P-ET)), indicating that reforestation under the SSP1-2.6 scenario leads to more P-ET than does the same reforestation under the SSP3-7.0 scenario over 52.9% of the global land. Among all 27 land regions, 10 regions show statistically significant Δ(δ(P-ET)) at the p = 0.10 level (bar plots in Figure 2D), and 9 of them are positive. Most of the positive Δ(δ(P-ET)) values are seen in America and Africa, with the largest difference being found in the Amazon (AMZ; 0.098 mm day^{-1}), followed by Central America (CAM; 0.070 mm day^{-1}) and East Africa (EAF; 0.057 mm day^{-1}). Although not statistically significant, substantial positive Δ(δ(P-ET)) values are also observed in Northeast Brazil (NEB) and East Asia (EAS). The changes in other regions are relatively minor, as shown in Figure S1B.

Figure S1C shows the LULCC of each region. It is shown that larger LULCC does not necessarily cause larger responses in P-ET. For instance, the psl fraction in NEB and West Africa (WAF) increases by 8.7% and 21.4%, respectively. δ(P-ET)$_{ssp126}$, however, shows limited changes. On the contrary, Alaska (ALA) does not have LULCC at all, but ALA shows substantial responses under both scenarios, and a statistically significant difference between the two scenarios (Figure S1B). These examples illustrate that the indirect effects of LULCC from remote regions and associated feedbacks are crucial in shaping local water availability. Another phenomenon is that, for some regions such as CAM, NEB, and WAF, δ(P-ET) is projected to decrease under both scenarios. In other words, reforestation in these regions does not bring hydrological benefits in terms of water availability. Figure S3 shows the model consistency of δ(P-ET)$_{ssp126}$, δ(P-ET)$_{ssp370}$, and their differences, in which number of models show the same sign of change as the MMM values, which are denoted by different colors. The regions with statistically significant changes usually have at least 5 models that agree on the sign of the MMM change, indicating that the signals identified here are robust and consistent across the models for most regions.

Figure S4 displays the spatial patterns of δP and δET under the two scenarios. Overall, the spatial pattern of δ(P-ET) is largely shaped by δP in both scenarios, and Δ(δ(P-ET)) is dominated by Δ(δP). To put it differently, the same level of reforestation causes different δP under different warming levels, which translates into different δ(P-ET). δET, nonetheless, is important in only a few regions, such as WAF under both scenarios and west North America (WNA) and east North America (ENA) under the SSP3-7.0 scenario.

Spatial and seasonal responses

The above analyses reveal an overall drying response of water availability to reforestation under the SSP3-7.0 scenario and a slightly wetting but statistically insignificant response under the SSP1-2.6 scenario. One intriguing question is how such responses manifest spatially and seasonally. To answer this question, we binned annual mean δ(P-ET) as a function of background P-ET in each scenario. The grids were sorted from the wettest to the driest based on the annual mean P-ET values in the background simulation at intervals of 10% in each model, in which 0%–10% represents the wettest 10% grids and 90%–100% represents the driest grids. Then, the area-weighted mean δ(P-ET) was calculated for each bin. Annually, δ(P-ET)$_{ssp126}$ shows moderate increases over the intervals between 20% and 60% and limited changes over other regions (Figure 3A, red). On the other hand, δ(P-ET)$_{ssp370}$ is negative across all bins (Figure 3A, blue). The largest decrease of δ(P-ET)$_{ssp370}$ is found in the wettest 30% grids, implying a "wet-gets-drier" pattern in space. Moreover, the largest difference between the two scenarios is mainly seen in the wet regions (e.g., the wettest 50% grids).

To examine their responses on a seasonal scale, we further binned δ(P-ET) as a function of background P-ET during wet and dry seasons, respectively. For a given grid, the wet (dry) season is defined as the wettest (driest) 3 consecutive months in the background simulation (methods). The slightly wetting response of annual δ(P-ET)$_{ssp126}$ is mainly contributed by the responses in the dry season, whereas the drying response of annual δ(P-ET)$_{ssp370}$, is dominated by the responses in the wet season (Figures 3B and 3C). In addition, the differences between δ(P-ET)$_{ssp126}$ and δ(P-ET)$_{ssp370}$ on an annual scale in the wet regions are mainly contributed by their differences in the wet season (Figure 3B), whereas during the dry season, their responses show limited differences (Figure 3C). A same analysis

Please cite this article in press as: Tang et al., Reforestation increases water inequality under low warming but reduces water availability under high warming, One Earth (2026), https://doi.org/10.1016/j.oneear.2026.101740

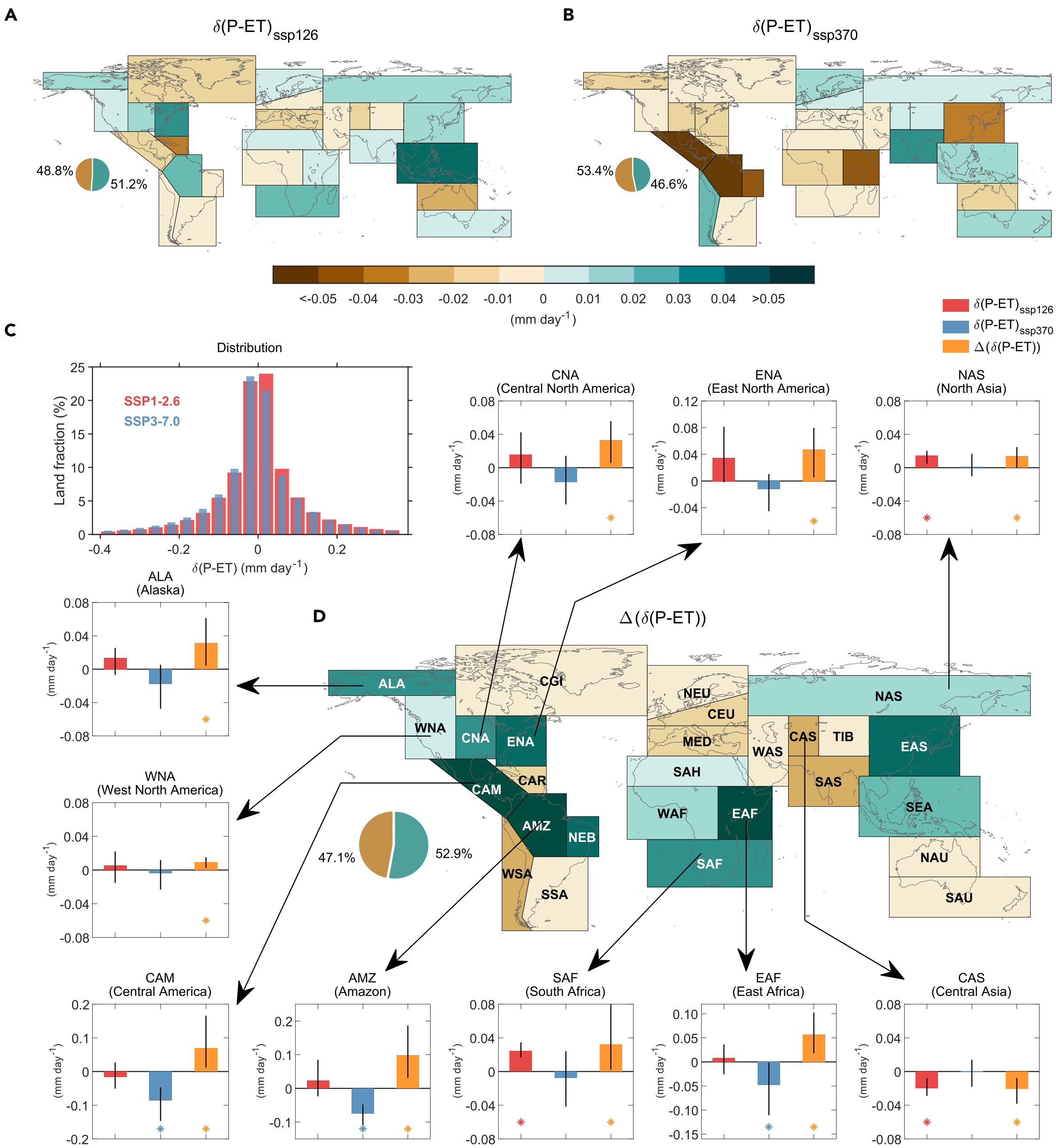

Figure 2. Regional responses of P-ET to reforestation

(A) Impact of reforestation on P-ET under the SSP1-2.6 scenario (denoted as $\delta(\text{P-ET})_{ssp126}$) for the 27 land regions. The pie chart denotes the land fractions with positive (green) and negative (brown) changes.

(B) Same as (A) but for the SSP3-7.0 scenario, denoted as $\delta(\text{P-ET})_{ssp370}$.

(C) Distribution plot for $\delta(\text{P-ET})_{ssp126}$ (red) and $\delta(\text{P-ET})_{ssp370}$ (blue).

(D) The central map portrays the regional differences in the impacts of reforestation between the two scenarios ($\delta(\text{P-ET})_{ssp126}$ minus $\delta(\text{P-ET})_{ssp370}$, denoted as $\Delta(\delta(\text{P-ET}))$, along with bar plots for 10 selected regions. The bars represent the MMM values, and the error bars represent the 90% confidence intervals (CIs). Asterisks denote that the changes are statistically significant at the p = 0.10 level.

was applied to δP and δET, and the results show that such spatial and seasonal shifts are largely shaped by δP instead of δET (Figure S5), revealing a dominating role of P in shaping water availability both spatially and temporally. These seasonal discrepancies are more obvious on a regional scale, which are shown in Figures 3D–3F and S6. The annual means $\delta(\text{P-ET})_{ssp126}$ and $\delta(\text{P-ET})_{ssp370}$ are largely the result of the competing effects of drying in the wet season and wetting in the dry season. Their differences on annual scale, $\Delta(\delta(\text{P-ET}))$, are mainly contributed by the wet season, especially over wet regions. The same analysis was performed based on growing and non-growing seasons, which are shown in Figures S7 and S8. For a given grid, the growing season is determined as the highest 6 consecutive months of leaf area index in the background simulation in each scenario. The differences over wet regions are contributed by both growing and non-growing seasons, with a slightly larger

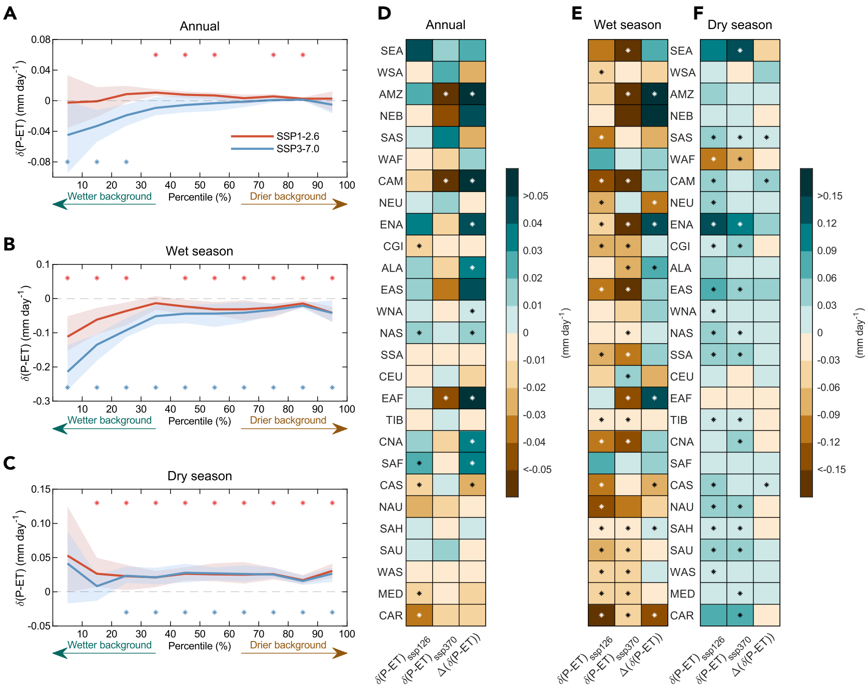

Figure 3. Spatial and seasonal responses of P-ET

(A) Annual mean δ(P-ET) as functions of background P-ET from the wettest grids (left) to the driest grids (right) at intervals of 10% for the SSP1-2.6 (red) and SSP3-7.0 scenarios (blue). The solid lines represent the MMM values, and the shades represent the 90% CIs. Red (blue) asterisks denote statistically significant changes at the p = 0.10 level for the SSP1-2.6 (SSP3-7.0) scenario.

(B and C) Same as (A) but for the wet season (B) and the dry season (C).

(D) Annual mean δ(P-ET) under the SSP1-2.6 scenario (left column), SSP3-7.0 scenario (middle column), and their differences (right column; SSP1-2.6 minus SSP3-7.0) for the 27 regions.

(E and F) Same as (D) but for the wet season (E) and the dry season (F). The regions in (D) and (F) are listed from the wettest (SEA) to the driest (CAR) based on the P-ET under the SSP1-2.6 scenario.

Asterisks in (D and F) indicate that the regional-mean changes are statistically significant at the p = 0.10 level.

role from the latter (Figure S8). The above analyses illustrate that reforestation under different warming levels not only impacts the mean water availability but also alters the spatial and seasonal distributions of water, providing additional evidence that the impacts of the same reforestation activity are distinct under contrasting warming levels.

Water availability per capita

Considering the changes in the water availability and spatial distributions, the next question is how such changes impact water availability in volume per capita. By the end of the 21st century, the global population is approximately 7.5 (12.2) billion under the SSP1-2.6 (SSP3-7.0) scenario, in which SSP3-7.0 has a larger population than that of SSP1-2.6 worldwide, except for North America and Europe (Figure S9). The differences in water availability in volume per capita between the two scenarios are shown in Figure 4A. The changes for each scenario and each region are shown in Figure S10, and the relative changes are shown in Figure S11. Generally, the spatial pattern of changes in P-ET in volume per capita is similar to that of mean P-ET shown in Figure 2, such as the increases in North America, Amazon, Africa, and East Asia, as well as the decreases in Europe (Figure 4A). This is not surprising, as the signs of change on P-ET per capita should be the same if the two scenarios had the same population. Different populations just amplify the differences in P-ET per capita, because the overall population size is smaller (larger) under the SSP1-2.6 (SSP3-7.0) scenario. Though much less populated and statistically insignificant, opposite changes are found in Canada/Greenland/Iceland (CGI) and North Australia (NAU). These two regions show negative Δ(δ(P-ET)) in the mean P-ET (Figure 2) but positive Δ(δ(P-ET)) in P-ET in volume per capita (Figure 4), implying a larger role from population differences than the changes in the mean P-ET.

To better understand how P-ET in volume per capita changes spatially, we again binned δ(P-ET) in volume per capita based on the background δ(P-ET) in volume per capita for the two scenarios. Reforestation under the SSP1-2.6 scenario causes an increase in P-ET in volume per capita in regions where P-ET per capita is already high, implying a ''rich-gets-richer'' response pattern, while reforestation under the SSP3-7.0 scenario causes an opposite response, in which the P-ET in volume per capita decreases in regions with high P-ET in volume per capita (Figure 4B). The largest changes are seen in the wettest 10% grids for both scenarios, in which P-ET in volume per capita increases (decreases) by 5.5×10^4 m^3 year^{-1} (5.4×10^4 m^3 year^{-1}) under the SSP1-2.6 (SSP3-7.0) scenario for the indicated amount, respectively. The magnitude of such changes gradually decreases when the background P-ET per capita gets smaller. One exception is that P-ET in volume per capita shows substantial reductions over the driest 10% grids under both scenarios.

Spatial inequality

The above analyses reveal that reforestation leads to different responses of water availability in space. For example, the wettest 20%–50% grids are projected to get wetter under the SSP1-2.6 scenario, whereas under the SSP3-7.0 scenario, a ''wet-gets-drier'' paradigm is observed (Figure 3A). To quantify how such shifts of spatial distribution impact the spatial inequality of P-ET, we further estimated the changes in the differences between the wettest and driest grids. For the mean δ(P-ET), the gap between the wettest 10% grids and driest 10% grids is projected to increase by 0.016 mm day^{-1} (Figure 5A, red), demonstrating an enhancement of spatial inequality between the wettest 10% and the driest 10% grids.

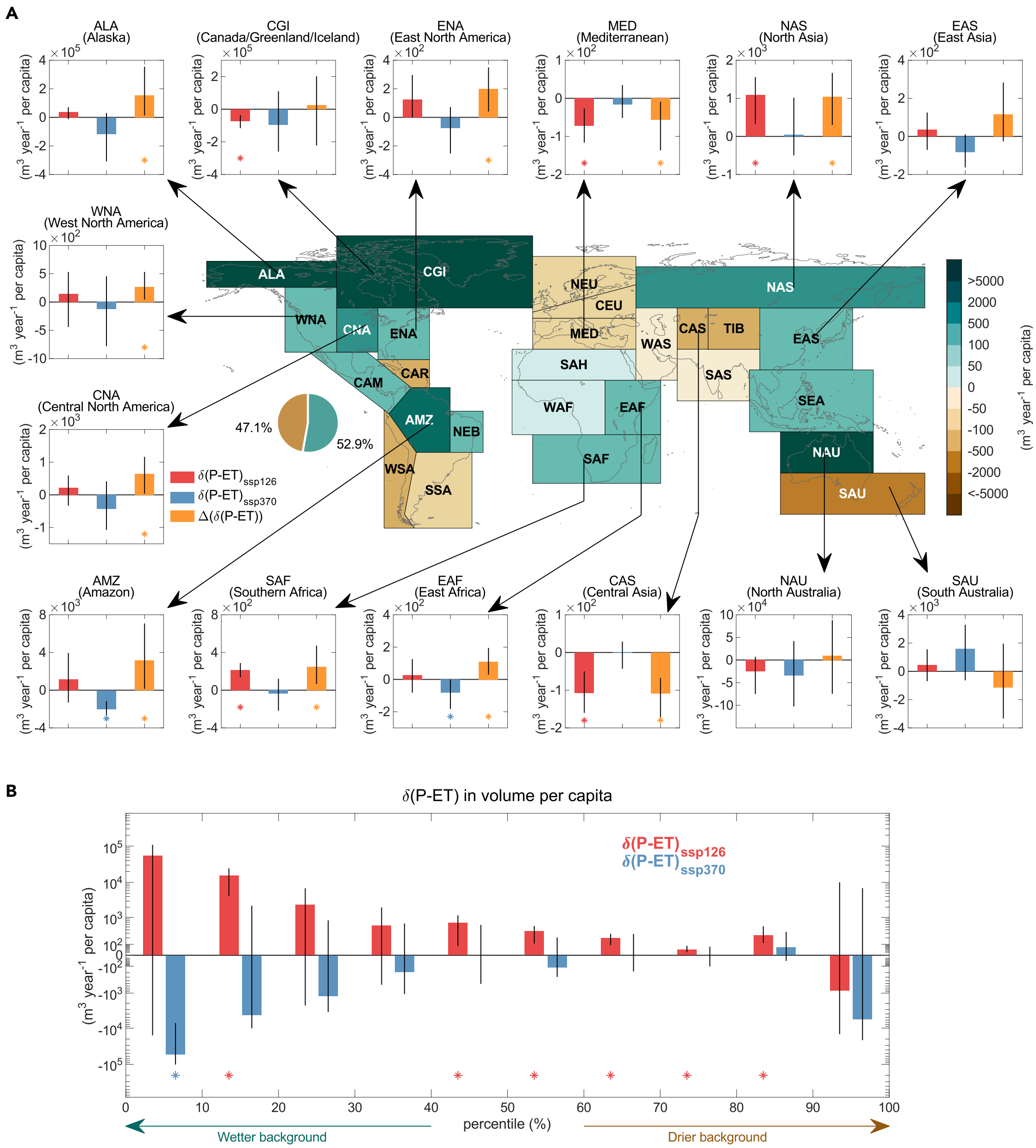

Figure 4. Differences of P-ET in volume per capita

(A) Regional differences of water availability in volume per capita (unit: m^3 $year^{-1}$) between the two scenarios ($\delta(P\text{-}ET)_{ssp126}$ minus $\delta(P\text{-}ET)_{ssp370}$ in volume per capita), along with bar plots for 14 selected regions. The pie chart denotes the land fractions with positive (green) and negative (brown) changes.

(B) δ(P-ET) in volume per capita as functions of background P-ET in volume per capita from the wettest grids (left) to the driest grids (right) at intervals of 10% for the SSP1-2.6 (red) and SSP3-7.0 scenarios (blue).

In both (A) and (B), the bars represent the MMM values, and the error bars represent the 90% confidence intervals (CIs). Asterisks denote statistically significant changes at the p = 0.10 level. Note the logarithmic scale on the y axis in (B).

Similar results are also observed for the remaining percentiles but with slightly reduced magnitudes as more grids are included. When all the grids are considered, the gap between the wettest 50% grids and the driest 50% grids is projected to increase by 0.009 mm day^{-1}, implying an overall exacerbation of spatial inequality. On the other hand, opposite changes are observed for the SSP3-7.0 scenario. The gaps between the wet and dry regions are projected to become smaller for all the percentiles examined (Figure 5A, blue), illustrating a reduced spatial inequality of water resources, with the largest reduction seen between the wettest 10% grids and the driest 10% grids (−0.015 mm day^{-1}).

When it comes to P-ET in volume per capita, similar results are found as those in the mean P-ET (Figure 5B). That is, the gaps between the wet and dry regions are projected to increase (decrease) under the SSP1-2.6 (SSP3-7.0) scenarios, thereby

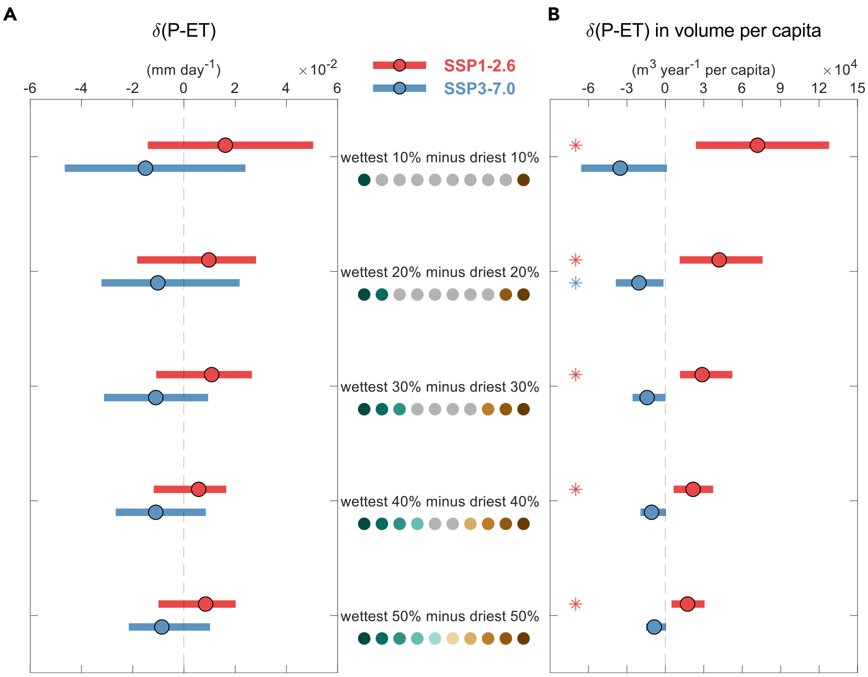

Figure 5. Changes in spatial inequality

(A) The differences of mean δ(P-ET) between the wettest and driest grids of the corresponding percentiles under SSP1-2.6 (red) and SSP3-7.0 scenarios (blue). The circles represent the MMM values, and the thick lines represent the 90% CIs. Asterisks denote statistically significant changes at the p = 0.10 level. Positive (negative) changes indicate enhanced (reduced) spatial inequality. The colored circles on the y axis label denote the fractions of grids for calculation, with each circle representing 10% of the grids from the wettest (dark green) to the driest (dark brown).

(B) Same as (A) but for δ(P-ET) in volume per capita.

enhancing (weakening) spatial inequality. All increases of the gaps under the SSP1-2.6 scenario are statistically significant at the p = 0.10 level, and the decrease of the gap between the wettest 20% grids and the driest 20% grids under the SSP3-7.0 scenario is also statistically significant. The largest increase (decrease) is again seen between the wettest 10% grids and driest 10% grids, and the magnitudes gradually decrease as more grids are included in the analyses.

Moisture budget analysis

The last question is why the same reforestation causes different responses in water availability. To answer this question, we first analyzed the circulation changes (shown in Figures 6A and 6B). It is seen that the circulation responses are quite divergent under the two scenarios. Taking tropical Africa as an example, the winds under the SSP1-2.6 scenario become more eastward, while under the SSP3-7.0 scenario, the winds show limited response. In fact, the wind responses at 500 hPa are distinct under the two scenarios over most of the globe. Changes in the geopotential height portray the same results. Different changes in the geopotential height can modify the pressure gradient, further influencing the circulation patterns.

To investigate the main factor driving the differences in δ(P-ET) under the two scenarios, a moisture budget analysis was performed. According to Seager et al.,[26] P-ET could be decomposed into four terms (methods). The first term is the dynamical term, representing the changes of P-ET contributed by mean circulation changes. The second term is the thermodynamical term, denoting the changes in P-ET due to humidity changes. The third term is the concomitant changes of both circulations and atmospheric humidity, which is usually referred to as nonlinear term. The last term is the residual, mainly transient eddies. We find that reforestation induces a strong nonlinear response under both scenarios, dominated by local wind-humidity coupling.

However, the dominant driver of Δ(δ(P-ET)) is primarily controlled by dynamic changes (Figure 6C). Among the 27 land regions, the dynamic term dominates the differences in 17 regions (blue), followed by nonlinear term in 8 regions (orange). All 9 regions with positive Δ(δ(P-ET)) identified in Figure 2C are dominated by the dynamic term except for North Asia (NAS). Besides, most differences in wet regions are also dominated by the dynamic term, except for western South America (WSA) and Southeast Asia (SEA), where the nonlinear term leads the changes. To sum up, the local wind-humidity coupling induced by reforestation is modulated by background circulation under different warming levels, making the mean circulation the dominant contributor to Δ(δ(P-ET)). It is worth noting that the purpose of Figures 6A and 6B is to illustrate the different responses in circulation under the two warming scenarios only. The detailed mechanisms of why circulations respond this way under each scenario merit future investigations.

DISCUSSION

The central knowledge gap motivating this study was whether the hydrological consequences of reforestation depend on the background climate state, a question that prior assessments did not fully answer because they either neglected indirect circulation feedbacks or assumed a static climate. To address this gap, we compared the impacts of the same idealized reforestation activity on land water availability (P-ET) under low- versus high-warming scenarios using the latest Earth system model simulations. Our objective was to determine whether reforestation produces divergent hydrological outcomes across climate states and, if so, to identify the possible mechanisms driving those differences. Our analysis reveals that the divergent P-ET responses are not simply a matter of magnitude but arise from fundamentally different circulation responses in wet regions (Figure 7). Under a low warming scenario, enhanced moisture convergence over wet regions amplifies the wet-gets-wetter pattern, increasing spatial inequality. Under a high warming scenario, by contrast, the background circulation weakens moisture flux, reducing both global mean P-ET and its spatial disparity. These contrasting circulation-driven patterns have direct

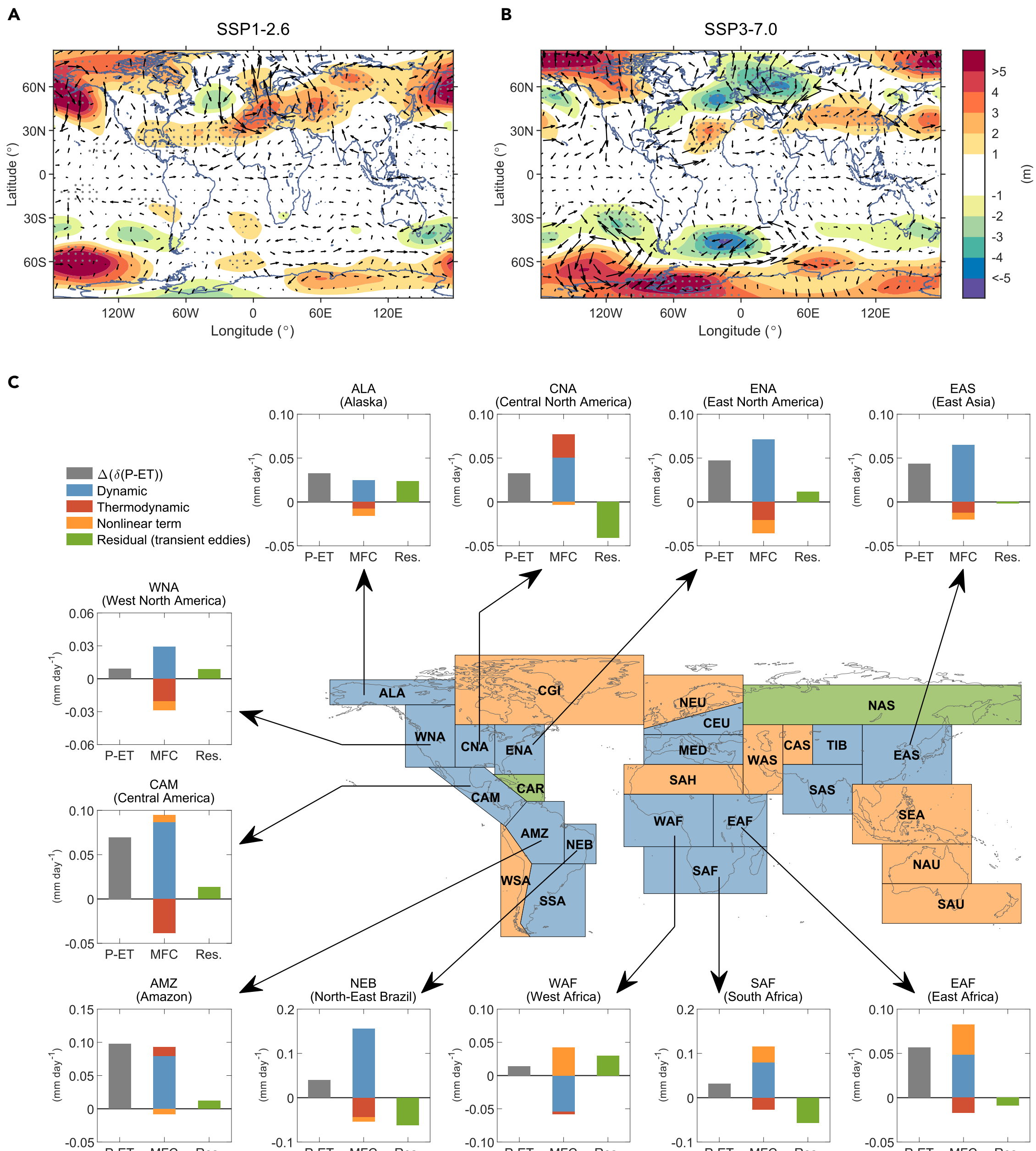

Figure 6. Circulation and moisture budget analysis

(A) Circulation responses to reforestation under the SSP1-2.6 scenario, with color shades representing the changes of geopotential height at 500 hPa and vectors representing the changes of winds at 500 hPa. Gray dots indicate that the changes of geopotential height are statistically significant at the $p = 0.10$ level, which are shown every 5 rows/columns.

(B) Same as (A) but for the SSP3-7.0 scenario.

(C) The central map shows the dominant driver, denoted by different color, for Δ(δ(P-ET)) in each region, and the bar plots show the contributions of each driver (mm day^{-1}) to Δ(δ(P-ET)) for selected regions. The P-ET term equals to the summation of the MFC and residual terms.

implications for ecosystem functioning: in the high-warming scenario, reduced water availability in wet regions could exacerbate water limitation, potentially reducing vegetation resilience[27,28] and carbon sequestration,[29] a feedback loop that current reforestation assessments rarely consider.

Direct quantitative comparisons between our results and previous studies are difficult due to different reforestation (e.g., location and magnitude), different background climate, and different treatments of indirect effects of LULCC.[11,14,15] The indirect effects of LULCC and associated feedbacks are fully considered in this study. The findings advance our understanding in three ways. First, while earlier studies reported that forests enhance precipitation and alleviate surface dryness under current climate conditions,[30,31] we show that this conclusion does not

Please cite this article in press as: Tang et al., Reforestation increases water inequality under low warming but reduces water availability under high warming, One Earth (2026), https://doi.org/10.1016/j.oneear.2026.101740

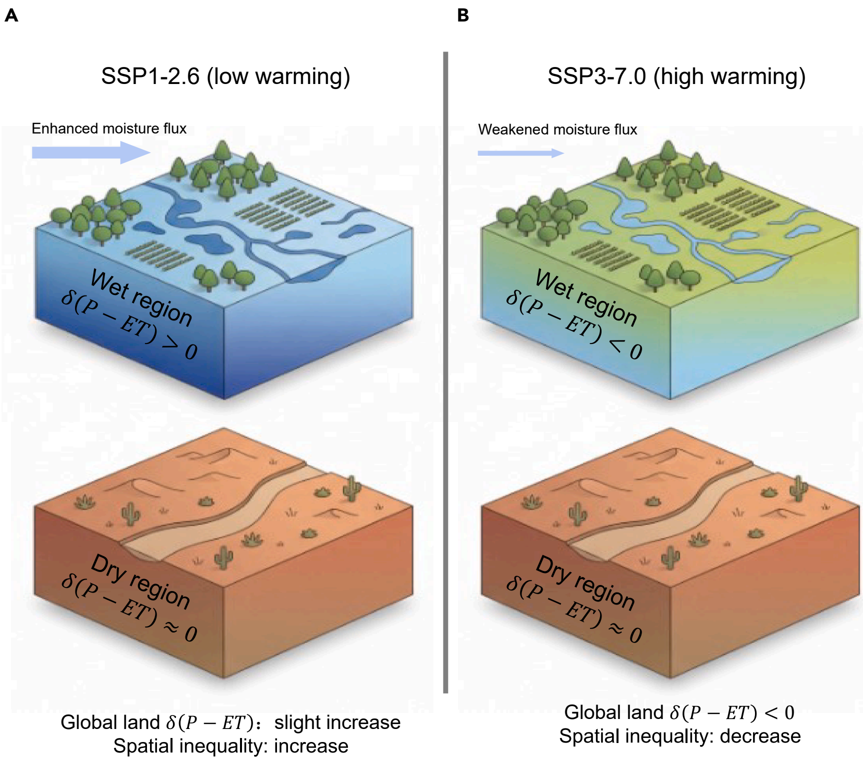

Figure 7. Conceptual illustration of divergent responses of P-ET to reforestation under low versus high warming

(A) Moisture transport is projected to enhance under the SSP1-2.6 scenario (low warming). Reforestation leads to a positive δ(P-ET) in the wet region (>0) and limited change in the dry region (≈0), resulting in an insignificant increase in global land-mean P-ET and an increase in spatial inequality.

(B) Moisture transport is substantially weakened under the SSP3-7.0 scenario (high warming). Reforestation leads to a negative δ(P-ET) in the wet region (<0) and limited change in the dry region (≈0), resulting in a net reduction in global land-mean P-ET (<0) and weakened spatial inequality.

automatically extend to a warmer world because the sign of the hydrological response can reverse, especially over wet regions. Second, by fully accounting for indirect circulation feedbacks, a factor many prior assessments overlooked, we demonstrate that the hydrological response to reforestation is fundamentally nonlinear, with the sign and magnitude of the P-ET change depending critically on the background climate state. Third, earlier studies disagreed on whether reforestation increases or decreases water availability.[32–34] We show that both sets of findings can be correct, as it all depends on the background climate states, a factor that previous work systematically ignored.

Several implications could be drawn from this study. First, for reforestation timing and background climate: the biophysical effects of forests on temperature have been reported to vary with background climate, including but not limited to latitude,[6,35] elevation,[36] CO_2 concentration,[18] and incoming radiation.[37] Our results demonstrate that the biophysical effects of reforestation on the hydrological cycle also vary with background climate, meaning that implementing the same reforestation program three decades earlier or later could produce significantly different outcomes, given that global mean temperature may rise by over 1 K within three decades under SSP3-7.0.[38] We therefore stress that background climate, reforestation timing, and other mitigation policies should be considered jointly in reforestation planning. Second, for transboundary governance and equity: our analyses reveal a crucial role of indirect effects of LULCC arising from changes in circulations and the background climate[23,39] (e.g., Figure 6). This implies that a country planning reforestation should consider not only hydrological effects within its borders but also remote consequences. Consequently, an inequality can emerge between LULCC performers and consequence sufferers. For example, WAF is projected to experience decreased water availability under both scenarios despite having the largest reforestation activity. This raises fundamental governance challenges: how to reconcile differing magnitudes of reforestation activity, investment, and outcomes across regions. Addressing this tension will require coordinated international policy frameworks, including benefit-sharing mechanisms and region-specific strategies, that explicitly account for the spatial redistribution of water resources. Third, for climate mitigation pathways: the strong dependence of hydrological outcomes on background climate means that the net sustainability value of reforestation is pathway-dependent. Under a high warming scenario, reforestation may carry hidden water costs—it may deplete water that is already scarce. Therefore, policymakers should not treat reforestation as a universally beneficial tool. Instead, its value depends on the emission scenario or how much warming we are facing.

Some limitations and uncertainties exist in this study. First, some land management practices, such as irrigation, wetland drainage, fire, and grazing, are not implemented in most of the current models,[40] and these processes can change the surface energy budget (including ET), as well as temperature, and may further modify P and ET.[41] Second, the current models are still unable to perfectly represent the biophysical effects of land cover changes, which may bias the simulated effects on ET[42,43] and, subsequently, P and P-ET.[44] An example is that both crop and grass are treated as grass in the models, but they may have different impacts on hydrological processes in reality.[45] Third, our reforestation scenario is not fully realistic. Taking the SSP370126Lu simulation as an example, it is not known whether the climate conditions under the SSP3-7.0 scenario can sustain such large-scale reforestation, as the deforestation/reforestation process, as well as global warming can significantly alter the local climate and ecological conditions,[46–50] potentially making some regions unsuitable for tree planting. Furthermore, whether tropical African countries can implement such large-scale reforestation, given their willingness, economy, and execution capacity, remains uncertain. Fourth, our results depend on the location of reforestation, which

Please cite this article in press as: Tang et al., Reforestation increases water inequality under low warming but reduces water availability under high warming, One Earth (2026), https://doi.org/10.1016/j.oneear.2026.101740

in this study mainly occurs in low latitudes (e.g., tropical Africa, Figure 1). Land-use change impacts are known to vary with location.[6,35,51,52] If reforestation were mainly in mid-latitudes, circulation responses and associated results are likely to differ. Lastly, while our results identify divergent circulation responses as the key driver of contrasting hydrological outcomes, a full mechanistic explanation, why the circulation responds oppositely under low versus high warming is beyond the scope of this study and warrants dedicated investigation in future work. Despite these limitations, our multi-model ensemble assessment provides robust evidence that reforestation impacts on water availability are strongly dependent on background climate, a finding that holds across the uncertainties we have examined.

These limitations point to several future research priorities to provide a more complete assessment. First, future studies should incorporate more realistic land management practices (irrigation, grazing, and fire regimes) and improved representations of biophysical processes. Second, reforestation scenarios should explore alternative spatial configurations (e.g., mid-latitude versus tropical and fragmented versus contiguous). Third, coupling Earth system models with integrated assessment models would allow exploration of socioeconomic feedbacks, including land-use competition and food security, under different mitigation pathways.

METHODS

CMIP6 model output

Seven models (one realization per model) from both the scenario model intercomparison project[24] and the land use model intercomparison project (LUMIP)[53] under the climate model intercomparison project phase 6 (CMIP6)[54] are employed in this study. For each model, four simulations are used to quantify the impact of the same level of reforestation under two developing pathways, which are summarized below.

	Simulation	TOA forcing	Land use scenario	Reforestation impact estimation
①	SSP370	SSP3-7.0	SSP3-7.0	②–①: isolate the impact of reforestation under the SSP3-7.0 scenario
②	SSP370126Lu	SSP3-7.0	SSP1-2.6	
③	SSP126	SSP1-2.6	SSP1-2.6	③–④: isolate the impact of the same reforestation under the SSP1-2.6 scenario
④	SSP126370Lu	SSP1-2.6	SSP3-7.0	

The 1^{st} simulation is the standard SSP370 simulation, which simulates the future climate from 2015 to 2100 in coupled mode with prescribed forcing under the shared socioeconomic pathway (SSP3-7.0). The SSP3-7.0 scenario represents a medium-to-high emission pathway with continued deforestation at current rates (Figure S1) and limited climate mitigation policies. The population decreases in industrialized countries but increases substantially in developing countries. Under this scenario, the radiative forcing is approximately 7.0 W m^{-2} at the top of the atmosphere (TOA) by the end of the 21^{st} century relative to 1850, and the global mean temperature is about 4 K warmer than the 1850 or 2.8 K warmer than the present level. The LULCC data are prescribed by the land-use harmonization dataset,[55] which is generated by integrated assessment models.[56] The 2^{nd} simulation SSP370126Lu is identical to the 1^{st} simulation, except that the LULCC data are from the SSP1-2.6 scenario. SSP1-2.6 represents the low-emission and sustainable developing pathway with strong climate mitigation policies and land use regulations, aiming to constrain the global mean temperature rise below 2 K by 2100 relative to the 1850 level. In this scenario, forests are substantially recovered at the expense of agricultural land (crop, pasture, and rangeland). The world population is similar to that of today. Thus, the SSP370126Lu simulation represents the reforestation version of the SSP3-7.0 scenario. By taking the difference between these two simulations (SSP370126Lu minus SSP370), the impact of reforestation under the SSP3-7.0 scenario is isolated. The differences between the two experiments are solely attributed to the biophysical effects of LULCC. The 3^{rd} and 4^{th} simulations are similar but are under the SSP1-2.6 scenario. The SSP126 simulation is the standard simulation under the SSP1-2.6 developing pathway, and SSP126370Lu is the deforestation version of SSP1-2.6, which has the same radiative forcing at the TOA as the SSP126 simulation but with LULCC from the SSP3-7.0 scenario. By taking the difference between these two simulations (SSP126 minus SSP126370Lu), the impact of the same reforestation under the SSP1-2.6 scenario was obtained. It is noted that these models were run in coupled mode; thus, the indirect effects of LULCC and associated atmospheric feedbacks are included in the results.

Model performance evaluation

To evaluate the performance of these CMIP6 models, we compared P, ET, and P-ET from the hist simulation against ERA5 reanalysis data. The comparison was performed based on the spatial pattern of 20-year mean values over 1995–2014 from ERA5 products and the CMIP6 output (Figure S12). In general, the models can reproduce the observed climatology reasonably well for all the variables examined. The correlation coefficients (r) between the MMM values of the CMIP6 models and ERA5 products are 0.89 for P, 0.94 for ET, and 0.80 for P-ET. In fact, the MMM values have the best performance in all three metrics and all three variables than any single model. For P-ET, the biases are within 1 mm day^{-1} over most of the land surface, except South America. In addition to the climatology, we also examined the trends of P-ET from the CMIP6 models in response to global warming over the historical period, including reforestation grids. The results demonstrate that the models could simulate the responses of P-ET to human activities fairly well (Figures S13 and S14; Note S1). Given this outcome, the selected models, especially in MMM values, are suitable for the analyses in the current study. More in-depth evaluations of these variables from the CMIP6 models are provided by Li et al.[57] (P), Wang et al.,[58] and Li et al.[59] (ET), as well as Allen[60] (P-ET) for the indicated variables.

Impact of reforestation on P-ET under each scenario

The reforestation impact under the SSP1-2.6 scenario, denoted as δ_{ssp126}, was quantified as the differences in the same variables between the two simulations with and without reforestation in each model. Taking P-ET as an example, the reforestation impact is defined as follows:

$$\delta(\mathrm{P}-\mathrm{ET})_{ssp126} = \overline{(P-ET)_{ssp126}} - \overline{(P-ET)_{SSP126370Lu}}. \quad \text{(Equation 1)}$$

In Equation 1, $\delta(\text{P-ET})_{ssp126}$ is the change in P-ET (unit: mm day^{-1}) due to reforestation under the SSP1-2.6 scenario, and the overbars represent the mean value during 2081–2100. The changes in other variables, such as P and ET, were estimated similarly by replacing P-ET in Equation 1 with the corresponding variables.

The impact of reforestation on P-ET (unit: mm day^{-1}) under the SSP3-7.0 scenario, denoted as $\delta(\text{P-ET})_{ssp370}$, was quantified similarly as:

$$\delta(\mathrm{P}-\mathrm{ET})_{ssp370} = \overline{(P-ET)_{ssp370126Lu}} - \overline{(P-ET)_{SSP370}}. \quad \text{(Equation 2)}$$

The reforestation is exactly the same under the two comparisons in Equations 1 and 2. The different impacts of the same reforestation on P-ET between these two scenarios, denoted by $\Delta(\delta)$, were estimated as follows:

$$\Delta(\delta(\mathrm{P}-\mathrm{ET})) = \delta(\mathrm{P}-\mathrm{ET})_{ssp126} - \delta(\mathrm{P}-\mathrm{ET})_{ssp370}. \quad \text{(Equation 3)}$$

$\delta(\text{P-ET})_{ssp126}$ and $\delta(\text{P-ET})_{ssp370}$ are the outputs from Equations 1 and 2, respectively. $\Delta(\delta(\text{P-ET}))$ represents the impact of different background climates. These differences were computed for each grid cell in each model and then averaged to obtain the MMM values, with an equal weighting factor assigned to each model. All model outputs were bilinearly resampled to a common spatial resolution of 0.94° × 1.25° in latitude and longitude before data processing.

Significance test and CI

A bootstrap technique was used to test whether the MMM values are significantly different from zero at the grid-cell level. The 7 model values were sampled 7 times randomly with replacement to obtain a mean value. The process was repeated 1,000 times to construct a 90% CI. The MMM changes are considered significant if zero falls outside the CI.

Area-weighted domain average

The model output is in a grid with equal latitude and longitude, meaning that the grid area decreases with increasing latitude. When calculating domain-averaged values, the value of each grid was weighted by the grid area. The weighting factor is approximated as *cosin(lat)*, where *lat* is the latitude of the grid. Only land grids are considered in the analyses.

Seasonal response

Wet (dry) season is defined as the consecutive 3 months featured with the maximum (minimum) P-ET value in the background climate for each grid in each model. The background climate is the climate of SSP126370Lu for SSP1-2.6 comparison and SSP370 simulations for SSP3-7.0 comparison, respectively.

Moisture budget analysis

According to Seager et al.,[26] P-ET on a monthly scale could be expressed as:

$$P-ET = -\frac{1}{\rho_w g}\int_0^{P_s} \nabla\cdot(\boldsymbol{u}q)dp, \quad \text{(Equation 4)}$$

where P and ET are monthly precipitation and evapotranspiration, respectively. ρ_w is the density of water (1,000 kg m^{-3}). $g$is the gravitational acceleration (9.8 m s^{-2}). Ps is the surface pressure (Pa). q is the specific humidity (kg kg^{-1}), and $\boldsymbol{u}$ is the horizontal wind vector (m s^{-1}). ∇denotes the horizontal divergence operator.

The right side of Equation 4 could be decomposed into two terms:

$$-\frac{1}{\rho_w g}\int_0^{P_s} \nabla\cdot(\boldsymbol{u}q)dp = -\frac{1}{\rho_w g}\int_0^{P_s} \nabla\cdot(\overline{\boldsymbol{u}}\overline{q})dp - \frac{1}{\rho_w g}\int_0^{P_s} \nabla\cdot(\overline{\boldsymbol{u}'q'})dp. \quad \text{(Equation 5)}$$

The first term on the right side of Equation 5 is the mean flow convergence (MFC), while the second term on the right side of Equation 5 is the transient eddy (TE). The overbars denote monthly mean values, while the primes denote deviations from the monthly mean values. Thus, the change in P-ET is the sum of changes in MFC and TE:

$$\delta(P-ET) = \delta MFC + \delta TE. \quad \text{(Equation 6)}$$

δMFC could be further approximated as:

$$\delta MFC = -\frac{1}{\rho_w g}\int_0^{P_s} \nabla\cdot(\overline{q}\delta\overline{\boldsymbol{u}})dp - \frac{1}{\rho_w g}\int_0^{P_s} \nabla\cdot(\overline{\boldsymbol{u}}\delta\overline{q})dp - \frac{1}{\rho_w g}\int_0^{P_s} \nabla\cdot(\delta\overline{q}\delta\overline{\boldsymbol{u}})dp. \quad \text{(Equation 7)}$$

The first term on the right side of Equation 7 represents the changes in MFC due to the changes in the mean circulation, which is referred to as the dynamic term. The second term on the right side of Equation 7 denotes the changes in MFC due to the changes in atmospheric humidity, which is referred to as the thermodynamic term. The third term is a covariant component of both circulations and humidity changes. Substituting Equations 5 and 7 into Equation 4 obtains:

$$\delta(P-ET) = -\frac{1}{\rho_w g}\int_0^{P_s} \nabla\cdot(\overline{q}\delta\overline{\boldsymbol{u}})dp - \frac{1}{\rho_w g}\int_0^{P_s} \nabla\cdot(\overline{\boldsymbol{u}}\delta\overline{q})dp - \frac{1}{\rho_w g}\int_0^{P_s} \nabla\cdot(\delta\overline{q}\delta\overline{\boldsymbol{u}})dp - \delta\frac{1}{\rho_w g}\int_0^{P_s} \nabla\cdot(\overline{\boldsymbol{u}'q'})dp. \quad \text{(Equation 8)}$$

The combination of the first three terms on the right side of Equation 8 is δMFC, while the last term on the right side of Equation 8 is δTE. The calculation of δTE requires hourly data. Due to the unavailability of such high-frequency data, δTE is estimated as the residual between δ(P-ET) and δMFC in this study. The calculation was performed for each pressure level and then integrated from the top of the atmosphere (pressure = 0) to the surface (pressure = P_s). The fractional contribution of each term is defined as the ratio of the absolute value of each term relative to the sum of all four terms in absolute value. The largest contributor is the term that has the maximum fractional contribution.

RESOURCE AVAILABILITY

Lead contact

Further information and requests for resources should be directed to and will be fulfilled by the lead contact, Tao Tang (tangtao@mail.iap.ac.cn).

Materials availability

This research did not generate new, unique materials.

Data and code availability

All data in this study are freely available from the web. The CMIP6 data are collected from the Earth System Grid Federation (ESGF) portal at https://esgf-node.llnl.gov/projects/cmip6/. LULCC data (LUH2) are downloaded from https://luh.umd.edu/. The shapefile defining the Intergovernmental Panel on Climate Change (IPCC) regions is downloaded from https://www.ipcc-data.org/guidelines/pages/ar5_regions.html. Population data for the SSP scenarios are collected from https://www.cgd.ucar.edu/sections/iam/modeling/spatial-population. The ERA-5 reanalysis products are downloaded from https://climate.copernicus.eu/climate-reanalysis. The MATLAB scripts used in this study are available upon reasonable request from the lead contact. The data for generating the figures in the main text are available at https://doi.org/10.5281/zenodo.20535362.

ACKNOWLEDGMENTS

T.T. acknowledges support from the Chinese Academy of Sciences (grant E663021601) and technical support of the National Large Scientific and Technological Infrastructure “Earth System Numerical Simulation Facility” (https://cstr.cn/31134.02.EL). J.G. acknowledges the support from the Natural Science Foundation of China (42375115). H.S. acknowledges the support from the Natural Science Foundation of China (42394132) and the National Key Technology R&D Program of China (2022YFC3201802). J.C. acknowledges the support from the Chinese Academy of Sciences (grant E354031801).

AUTHOR CONTRIBUTIONS

T.T. and J.G. conceived the study. T.T. collected the data, carried out the data analyses, and wrote the initial manuscript. All authors contributed to results framing, scientific discussion, and manuscript revision.

DECLARATION OF INTERESTS

The authors declare no competing interests.

SUPPLEMENTAL INFORMATION

Supplemental information can be found online at https://doi.org/10.1016/j.oneear.2026.101740.

Received: August 18, 2025
Revised: December 1, 2025
Accepted: May 20, 2026

REFERENCES

1. Griscom, B.W., Adams, J., Ellis, P.W., Houghton, R.A., Lomax, G., Miteva, D.A., Schlesinger, W.H., Shoch, D., Siikamäki, J.V., Smith, P., et al. (2017). Natural climate solutions. Proc. Natl. Acad. Sci. USA *114*, 11645–11650. https://doi.org/10.1073/pnas.1710465114.
2. Lewis, S.L., Wheeler, C.E., Mitchard, E.T.A., and Koch, A. (2019). Restoring natural forests is the best way to remove atmospheric carbon. Nature *568*, 25–28. https://doi.org/10.1038/d41586-019-01026-8.
3. Liang, S., Liang, L., Wang, D., and Zeng, Z. (2024). Dryland forestation: Uncovering the carbon sequestration potential. Innov. Geosci. *2*, 100058. https://doi.org/10.59717/j.xinn-geo.2024.100058.
4. Bonan, G.B. (2008). Forests and Climate Change: Forcings, Feedbacks, and the Climate Benefits of Forests. Science *320*, 1444–1449. https://doi.org/10.1126/science.1155121.
5. Pan, Y., Birdsey, R.A., Fang, J., Houghton, R., Kauppi, P.E., Kurz, W.A., Phillips, O.L., Shvidenko, A., Lewis, S.L., Canadell, J.G., et al. (2011). A Large and Persistent Carbon Sink in the World’s Forests. Science *333*, 988–993. https://doi.org/10.1126/science.1201609.
6. Lee, X., Goulden, M.L., Hollinger, D.Y., Barr, A., Black, T.A., Bohrer, G., Bracho, R., Drake, B., Goldstein, A., Gu, L., et al. (2011). Observed increase in local cooling effect of deforestation at higher latitudes. Nature *479*, 384–387. https://doi.org/10.1038/nature10588.
7. Winckler, J., Reick, C.H., Bright, R.M., and Pongratz, J. (2019). Importance of Surface Roughness for the Local Biogeophysical Effects of Deforestation. JGR. Atmospheres *124*, 8605–8618. https://doi.org/10.1029/2018JD030127.
8. Staal, A., Tuinenburg, O.A., Bosmans, J.H.C., Holmgren, M., van Nes, E.H., Scheffer, M., Zemp, D.C., and Dekker, S.C. (2018). Forest-rainfall cascades buffer against drought across the Amazon. Nat. Clim. Change *8*, 539–543. https://doi.org/10.1038/s41558-018-0177-y.
9. Tuinenburg, O.A., Bosmans, J.H.C., and Staal, A. (2022). The global potential of forest restoration for drought mitigation. Environ. Res. Lett. *17*, 034045. https://doi.org/10.1088/1748-9326/ac55b8.
10. Tang, T., Ge, J., Cao, J., and Shi, H. (2025). Land water availability altered by historical land use and land cover change. npj Clim. Atmos. Sci. *8*, 230. https://doi.org/10.1038/s41612-025-01111-y.
11. Sterling, S.M., Ducharne, A., and Polcher, J. (2013). The impact of global land-cover change on the terrestrial water cycle. Nat. Clim. Change *3*, 385–390. https://doi.org/10.1038/nclimate1690.
12. Zhao, M., A, G., Zhang, J., Velicogna, I., Liang, C., and Li, Z. (2020). Ecological restoration impact on total terrestrial water storage. Nat. Sustain. *4*, 56–62. https://doi.org/10.1038/s41893-020-00600-7.
13. Engel, F., Hoek van Dijke, A.J., Roebroek, C.T.J., and Benedict, I. (2025). Can large-scale tree cover change negate climate change impacts on future water availability? Hydrol. Earth Syst. Sci. *29*, 1895–1918. https://doi.org/10.5194/hess-29-1895-2025.
14. Zan, B., Ge, J., Mu, M., Sun, Q., Luo, X., and Wei, J. (2024). Spatiotemporal inequality in land water availability amplified by global tree restoration. Nat. Water *2*, 863–874. https://doi.org/10.1038/s44221-024-00296-5.
15. Hoek van Dijke, A.J., Herold, M., Mallick, K., Benedict, I., Machwitz, M., Schlerf, M., Pranindita, A., Theeuwen, J.J.E., Bastin, J.F., and Teuling, A.J. (2022). Shifts in regional water availability due to global tree restoration. Nat. Geosci. *15*, 363–368. https://doi.org/10.1038/s41561-022-00935-0.
16. Fu, Q., Shi, R., Li, T., Sun, Y., Liu, D., Cui, S., and Hou, R. (2019). Effects of land-use change and climate variability on streamflow in the Woken River basin in Northeast China. River Res. Appl. *35*, 121–132. https://doi.org/10.1002/rra.3397.
17. Zhang, L., Zhao, F., Chen, Y., and Dixon, R.N.M. (2011). Estimating effects of plantation expansion and climate variability on streamflow for catchments in Australia. Water Resour. Res. *47*. https://doi.org/10.1029/2011WR010711.
18. Pitman, A.J., Avila, F.B., Abramowitz, G., Wang, Y.P., Phipps, S.J., and de Noblet-Ducoudré, N. (2011). Importance of background climate in determining impact of land-cover change on regional climate. Nat. Clim. Change *1*, 472–475. https://doi.org/10.1038/nclimate1294.
19. Bonan, G.B., Pollard, D., and Thompson, S.L. (1992). Effects of boreal forest vegetation on global climate. Nature *359*, 716–718. https://doi.org/10.1038/359716a0.
20. Luo, X., Ge, J., Cao, Y., Liu, Y., Yang, L., Wang, S., and Guo, W. (2024). Local and Nonlocal Biophysical Effects of Historical Land Use and Land Cover

Changes in CMIP6 Models and the Intermodel Uncertainty. Earths Future *12*, e2023EF004220. https://doi.org/10.1029/2023EF004220.

21. Ma, S., Zhou, S., Yu, B., and Song, J. (2024). Deforestation-induced runoff changes dominated by forest-climate feedbacks. Sci. Adv. *10*, eadp3964. https://doi.org/10.1126/sciadv.adp3964.

22. Tang, T., Lee, X., and Zhang, K. (2024). Historical land use and land cover change reduced the temperature of cold extremes more than that of hot extremes. Innov. Geosci. *2*, 100079. https://doi.org/10.59717/j.xinn-geo.2024.100079.

23. Portmann, R., Beyerle, U., Davin, E., Fischer, E.M., De Hertog, S., and Schemm, S. (2022). Global forestation and deforestation affect remote climate via adjusted atmosphere and ocean circulation. Nat. Commun. *13*, 5569. https://doi.org/10.1038/s41467-022-33279-9.

24. O'Neill, B.C., Tebaldi, C., van Vuuren, D.P., Eyring, V., Friedlingstein, P., Hurtt, G., Knutti, R., Kriegler, E., Lamarque, J.F., and Lowe, J. (2016). The Scenario Model Intercomparison Project (ScenarioMIP) for CMIP6. Geosci. Model Dev. *9*, 3461–3482. https://doi.org/10.5194/gmd-9-3461-2016.

25. Seneviratne, S.I., et al. (2012). In A Special Report of Working Groups I and II of the Intergovernmental Panel on Climate Change (IPCC), C.B. Field, et al., eds. (Cambridge University Press), pp. 1–7.

26. Seager, R., Ting, M., Held, I., Kushnir, Y., Lu, J., Vecchi, G., Huang, H.P., Harnik, N., Leetmaa, A., Lau, N.C., et al. (2007). Model projections of an imminent transition to a more arid climate in southwestern North America. Science *316*, 1181–1184. https://doi.org/10.1126/science.1139601.

27. Smith, T., and Boers, N. (2023). Global vegetation resilience linked to water availability and variability. Nat. Commun. *14*, 498. https://doi.org/10.1038/s41467-023-36207-7.

28. Xu, H., Pang, J., Chen, J., Wei, X., Wu, X., Cao, W., Yuan, Z., Sun, G., Xu, Y., Zhang, Q., and Zhang, Z. (2025). Water Budgets Control the Resilience of Large-Scale Ecological Restoration. Geophys. Res. Lett. *52*, e2025GL116914. https://doi.org/10.1029/2025GL116914.

29. Zhao, Z., Zhou, Y., Ju, W., Xiao, J., and Li, X. (2025). Widespread and Divergent Post-Drought Loss of Gross Primary Production. Geophys. Res. Lett. *52*, e2025GL115825. https://doi.org/10.1029/2025GL115825.

30. Smith, C., Baker, J.C.A., and Spracklen, D.V. (2023). Tropical deforestation causes large reductions in observed precipitation. Nature *615*, 270–275. https://doi.org/10.1038/s41586-022-05690-1.

31. Staal, A., Theeuwen, J.J.E., Wang-Erlandsson, L., Wunderling, N., and Dekker, S.C. (2024). Targeted rainfall enhancement as an objective of forestation. Glob. Change Biol. *30*, e17096. https://doi.org/10.1111/gcb.17096.

32. Liu, Y., Li, Z., Chen, Y., Jin, L., Li, F., Wang, X., Long, Y., Liu, C., and Kayumba, P.M. (2025). Global greening drives significant soil moisture loss. Commun. Earth Environ. *6*, 600. https://doi.org/10.1038/s43247-025-02470-3.

33. Li, Z., Liu, W., Wang, T., Wang, H., Feng, Y., Tang, S., and Sun, F. (2025). Biophysical Impacts of Earth Greening Modulate Average and Extreme Water Availability. Geophys. Res. Lett. *52*, e2025GL117797. https://doi.org/10.1029/2025GL117797.

34. Zeng, Z., Piao, S., Li, L.Z.X., Wang, T., Ciais, P., Lian, X., Yang, Y., Mao, J., Shi, X., and Myneni, R.B. (2018). Impact of Earth Greening on the Terrestrial Water Cycle. J. Clim. *31*, 2633–2650. https://doi.org/10.1175/JCLI-D-17-0236.1.

35. Tang, T., Lee, X., Zhang, K., Cai, L., Lawrence, D.M., and Shevliakova, E. (2023). Biophysical Impact of Land-Use and Land-Cover Change on Subgrid Temperature in CMIP6 Models. J. Hydrometeorol. *24*, 373–388. https://doi.org/10.1175/JHM-D-22-0073.1.

36. Zeng, Z., Wang, D., Yang, L., Wu, J., Ziegler, A.D., Liu, M., Ciais, P., Searchinger, T.D., Yang, Z.L., Chen, D., et al. (2021). Deforestation-induced warming over tropical mountain regions regulated by elevation. Nat. Geosci. *14*, 23–29. https://doi.org/10.1038/s41561-020-00666-0.

37. Ge, J., Huang, X., Zan, B., Qiu, B., Cao, Y., and Guo, W. (2023). Local surface cooling from afforestation amplified by lower aerosol pollution. Nat. Geosci. *16*, 781–788. https://doi.org/10.1038/s41561-023-01251-x.

38. IPCC. (2021). In Climate change 2021: the physical science basis. Contribution of Working Group I to the Sixth Assessment Report of the Intergovernmental Panel on Climate Change, V. Masson-Delmotte, et al., eds. (Cambridge University Press), pp. 3–32.

39. Wang-Erlandsson, L., Fetzer, I., Keys, P.W., van der Ent, R.J., Savenije, H.H.G., and Gordon, L.J. (2018). Remote land use impacts on river flows through atmospheric teleconnections. Hydrol. Earth Syst. Sci. *22*, 4311–4328. https://doi.org/10.5194/hess-22-4311-2018.

40. Pongratz, J., Dolman, H., Don, A., Erb, K., Fuchs, R., Herold, M., Jones, C., Kuemmerle, T., Luyssaert, S., Meyfroidt, P., and Naudts, K. (2018). Models meet data: Challenges and opportunities in implementing land management in Earth system models. Glob. Change Biol. *24*, 1470–1487. https://doi.org/10.1111/gcb.13988.

41. McDermid, S., Nocco, M., Lawston-Parker, P., Keune, J., Pokhrel, Y., Jain, M., Jägermeyr, J., Brocca, L., Massari, C., Jones, A.D., et al. (2023). Irrigation in the Earth system. Nat. Rev. Earth Environ. *4*, 435–453. https://doi.org/10.1038/s43017-023-00438-5.

42. Luo, X., Ge, J., Guo, W., Cao, Y., Liu, Y., Chen, C., and Yang, L. (2023). An Evaluation of CMIP6 Models in Representing the Biophysical Effects of Deforestation With Satellite-Based Observations. JGR. Atmospheres *128*, e2022JD038198. https://doi.org/10.1029/2022JD038198.

43. Ge, J., Qiu, B., Chu, B., Li, D., Jiang, L., Zhou, W., Tang, J., and Guo, W. (2021). Evaluation of Coupled Regional Climate Models in Representing the Local Biophysical Effects of Afforestation over Continental China. J. Clim. *34*, 1–62. https://doi.org/10.1175/JCLI-D-21-0462.1.

44. Luo, X., Ge, J., Guo, W., Fan, L., Chen, C., Liu, Y., and Yang, L. (2022). The Biophysical Impacts of Deforestation on Precipitation: Results from the CMIP6 Model Intercomparison. J. Clim. *35*, 3293–3311. https://doi.org/10.1175/JCLI-D-21-0689.1.

45. Twine, T.E., Kucharik, C.J., and Foley, J.A. (2004). Effects of Land Cover Change on the Energy and Water Balance of the Mississippi River Basin. J. Hydrometeorol. *5*, 640–6655. https://doi.org/10.1175/1525-7541(2004)005<0640:EOLCCO>2.0.CO;2.

46. Feng, X., Fu, B., Piao, S., Wang, S., Ciais, P., Zeng, Z., Lü, Y., Zeng, Y., Li, Y., Jiang, X., and Wu, B. (2016). Revegetation in China's Loess Plateau is approaching sustainable water resource limits. Nat. Clim. Change *6*, 1019–1022. https://doi.org/10.1038/nclimate3092.

47. Tang, T., Ge, J., Shi, H., and Cao, J. (2025). Divergent response of aridity index to historical land use and land cover change. npj Clim. Atmos. Sci. *8*, 88. https://doi.org/10.1038/s41612-025-00978-1.

48. Xu, X., Zhang, X., Riley, W.J., Xue, Y., Nobre, C.A., Lovejoy, T.E., and Jia, G. (2022). Deforestation triggering irreversible transition in Amazon hydrological cycle. Environ. Res. Lett. *17*, 034037. https://doi.org/10.1088/1748-9326/ac4c1d.

49. Huang, J., Yu, H., Guan, X., Wang, G., and Guo, R. (2016). Accelerated dryland expansion under climate change. Nat. Clim. Change *6*, 166–171. https://doi.org/10.1038/nclimate2837.

50. Tang, T., Ge, J., Shi, H., Wang, L., Cao, J., and Lee, X. (2025). Drought frequency, intensity, and exposure have increased due to historical land use and land cover changes. Commun. Earth Environ. *6*, 398. https://doi.org/10.1038/s43247-025-02392-0.

51. Perugini, L., Caporaso, L., Marconi, S., Cescatti, A., Quesada, B., de Noblet-Ducoudré, N., House, J.I., and Arneth, A. (2017). Biophysical effects on temperature and precipitation due to land cover change. Environ. Res. Lett. *12*, 053002. https://doi.org/10.1088/1748-9326/aa6b3f.

52. Fahrenbach, N.L.S., De Hertog, S.J., Jäger, F., Lawrence, P.J., and Jnglin Wills, R.C. (2026). Reforestation scenarios shape global and regional temperature outcomes. Commun. Earth Environ. *7*, 204. https://doi.org/10.1038/s43247-026-03331-3.

53. Lawrence, D.M., Hurtt, G.C., Arneth, A., Brovkin, V., Calvin, K.V., Jones, A.D., Jones, C.D., Lawrence, P.J., de Noblet-Ducoudré, N., Pongratz,

J., et al. (2016). The Land Use Model Intercomparison Project (LUMIP) contribution to CMIP6: rationale and experimental design. Geosci. Model Dev. *9*, 2973–2998. https://doi.org/10.5194/gmd-9-2973-2016.

54. Eyring, V., Bony, S., Meehl, G.A., Senior, C.A., Stevens, B., Stouffer, R.J., and Taylor, K.E. (2016). Overview of the Coupled Model Intercomparison Project Phase 6 (CMIP6) experimental design and organization. Geosci. Model Dev. *9*, 1937–1958. https://doi.org/10.5194/gmd-9-1937-2016.

55. Hurtt, G.C., Chini, L., Sahajpal, R., Frolking, S., Bodirsky, B.L., Calvin, K., Doelman, J.C., Fisk, J., Fujimori, S., Klein Goldewijk, K., et al. (2020). Harmonization of global land use change and management for the period 850–2100 (LUH2) for CMIP6. Geosci. Model Dev. *13*, 5425–5464. https://doi.org/10.5194/gmd-13-5425-2020.

56. Riahi, K., van Vuuren, D.P., Kriegler, E., Edmonds, J., O'Neill, B.C., Fujimori, S., Bauer, N., Calvin, K., Dellink, R., Fricko, O., et al. (2017). The Shared Socioeconomic Pathways and their energy, land use, and greenhouse gas emissions implications: An overview. Glob. Environ. Change *42*, 153–168. https://doi.org/10.1016/j.gloenvcha.2016.05.009.

57. Li, Z., Liu, T., Huang, Y., Peng, J., and Ling, Y. (2022). Evaluation of the CMIP6 Precipitation Simulations Over Global Land. Earths Future *10*, e2021EF002500. https://doi.org/10.1029/2021EF002500.

58. Wang, Z., Zhan, C., Ning, L., and Guo, H. (2021). Evaluation of global terrestrial evapotranspiration in CMIP6 models. Theor. Appl. Climatol. *143*, 521–531. https://doi.org/10.1007/s00704-020-03437-4.

59. Li, J., Miao, C., Wei, W., Zhang, G., Hua, L., Chen, Y., and Wang, X. (2021). Evaluation of CMIP6 Global Climate Models for Simulating Land Surface Energy and Water Fluxes During 1979–2014. J. Adv. Model. Earth Syst. *13*, e2021MS002515. https://doi.org/10.1029/2021MS002515.

60. Allan, R.P. (2023). Amplified seasonal range in precipitation minus evaporation. Environ. Res. Lett. *18*, 094004. https://doi.org/10.1088/1748-9326/acea36.